Determination of the Radiative Properties of the TiO_2 Porous Thin Films in the UV-VIS Spectral Range

Rui Qi, Rong Chen, Junming Zhao, Qiang Liao, Xun Zhu, and Dingding Ye

Abstract TiO_2 porous thin film has been widely used as the photoanode of the photocatalytic fuel cell. The distribution of the light intensity in this type of the photoanode greatly affects its performance, which can be obtained by solving the radiative transfer equation. Under this circumstance, the determination of the radiative properties of the TiO_2 porous thin films is crucial. In this work, based on the measured thickness, the normal-hemispherical reflectance and transmittance of the porous thin films, the absorption coefficient and scattering coefficient were determined by using the spectral element method. It was found that the TiO_2 porous thin films exhibited high scattering coefficient and relatively low absorption coefficient. The absorption coefficient sharply decreased in the UV region with increasing the wavelength and then was almost unchanged in the visible-light range. The scattering coefficient firstly increased and then decreased. There existed a maximum scattering coefficient at a wavelength of about 378 nm. Moreover, the effect of the porosity was investigated by adding the pore former of PMMA in the porous thin film. The results indicated that the scattering coefficient remarkably increased with increasing the porosity, while the absorption coefficient was insensitive to the porosity variation.

Keywords TiO_2 porous thin films · Porosity · Reflectance and transmittance · Absorption and scattering coefficients · Spectral element method

R. Qi · R. Chen (✉) · Q. Liao · X. Zhu · D. Ye
Key Laboratory of Low-Grade Energy Utilization Technologies and Systems, Chongqing University, Ministry of Education, Chongqing 400030, China
e-mail: rchen@cqu.edu.cn

R. Qi · R. Chen · Q. Liao · X. Zhu · D. Ye
Institute of Engineering Thermophysics, School of Energy and Power Engineering, Chongqing University, Chongqing 400030, China

J. Zhao (✉)
School of Energy Science and Engineering, Harbin Institute of Technology, Harbin 150001, China
e-mail: jmzhao@hit.edu.cn

S. N. Atluri and I. Vušanović (eds.), *Computational and Experimental Simulations in Engineering*, Mechanisms and Machine Science 98,
https://doi.org/10.1007/978-3-030-67090-0_9

1 Introduction

In recent years, photocatalytic fuel cells that combine the advantages of both the photocatalytic and fuel cell technologies, have received increasing attention, because they can directly convert chemical energy stored in wastewater into electricity via the photoelectrochemical reactions [1–4]. This new technology has exhibited significant potentials in the sewage treatment and the production of clean energy simultaneously. Although photocatalytic fuel cells have been widely investigated, there are still many problems to be solved, such as low photonic efficiency, serious electron-hole recombination, low photocurrent density, and low power output, etc. These problems are clearly related to the photoanode so that extensive efforts have been devoted to the development of high-performance photoanode. Actually, the transport characteristics in the photoanode also greatly affect its performance because the reactant/product, light, ion, electron and hole simultaneously transport in the photoanode and are coupled with the photoelectrochemical reactions. Unfortunately, the transport mechanism still remains unclear, such as the light transfer, which restricts further development of the photoanode.

One of the approaches to understand the transport characteristics in the photoanode is the simulation method. In particular, the light transport, which is a primary factor for initiating the photoelectrochemical reaction in the photoanode, significantly affects the accuracy of the simulation. In conventional, an empirical formula has been widely used to simulate the light transport in the photoanode [5–7]. Although the empirical formula is simple and easy to be incorporated into the model, it is unable to objectively describe the light transport in the photoanode because the influence of light scattering is ignored but considerably strong in the nano-porous structure [8]. Hence, to develop a more accurate transport model for the photoanode, it is essential to accurately describe the distribution of light intensity in the photoanode. Solving the radiative transport equation (RTE) is one of the best methods. However, in order to solve this equation, two important radiative parameters must be obtained, namely the absorption coefficient and the scattering coefficient of the photoanode. Currently, these two parameters of the photoanode are unavailable, limiting the development of the transport model.

In fact, there exist many methods to determine the radiative parameters of porous media. In 1984, Makino et al. [9] obtained the absorption coefficients and scattering coefficients of ceramics materials using the Kubelka–Munk method. Subsequently, Molenaar et al. [10] applied this method to other porous media. Meanwhile, Pickering et al. and Cheong et al. [11, 12] used the inverse adding-doubling (IAD) method to estimate the optical properties of various biological tissues by the experimentally determined reflectance and transmittance. At present, this method has been widely used in the calculation of optical parameters of chaotic media. In 2006, Petrasch et al. [13] calculated the radiative properties such as the extinction coefficient and scattering phase functions of porous media by Monte Carlo method. Xie et al. [14] also utilized this method to investigate the radiative properties of ZnO particles and ZnO-Au composite particles in suspension.

In addition, Morales et al. [15] used the spectral element method to determine the reflection and transmission coefficients of collimated light in a multiple slabs. Overall, although there are many works on the determination of radiative parameters of porous media, far too little attention has been paid to the radiative properties of the TiO_2 porous thin films.

In this work, therefore, we prepared typical porous thin films using the commercial TiO_2 nanoparticles, which have been widely used in the photoanode. The normal-hemispherical reflectance, normal-hemispherical transmittance and thicknesses of the TiO_2 porous thin films were measured, which were then employed to retrieve the radiative properties, i.e., the absorption coefficient and the scattering coefficient of the porous thin film. During the retrieving, the RTE was solved using the spectral element method [16] and combined with the Levenberg-Marquardt algorithm. On the other hand, the effect of porosity on the variation of the spectral absorption and scattering coefficients was also examined. The achieved results are helpful for further experimental and theoretical research on the transport characteristics of the TiO_2 porous thin films with the consideration of the microstructural effect on the photoanode.

2 Experimental Section

2.1 Preparation of Typical TiO_2 Porous Thin Films

In this work, the typical TiO_2 porous thin films were prepared on the glass slides by the wet spraying method with the TiO_2 colloid [17]. To prepare the colloid, 12 g of TiO_2 commercial nanoparticles (Aeroxide P25, Acros, Belgium) were firstly dispersed to 120 mL of deionized water before adding 0.4 mL acetylacetone (Kelong Chemical Reagent Factory, China). After that, 0.2 mL of Triton X-100 (Solibao Technology, China) and 2.4 g of polyethylene glycol (Kelong Chemical Reagent Factory, China) were added to the mixed solution and continuously stirred in a magnetic stirrer for 12 h. The well-prepared TiO_2 colloid was diluted with ethanol and sprayed on the glass slide by an air spray gun. Finally, the samples were calcined at 550 °C for 2 h to obtain the TiO_2 porous thin films with different loadings, about 0.5 mg/cm^2, 1.0 mg/cm^2, 2.0 mg/cm^2, and 3.0 mg/cm^2, respectively.

2.2 Preparation of TiO_2 Porous Thin Films with Pore Formers

The TiO_2 porous thin films with pore formers were prepared by using TiO_2 colloid and adding the pore formers of PMMA microspheres (Ruige Technology, China) with 1 μm in diameter as templates [18]. First, the aqueous solution of polyvinyl

alcohol (1 wt%) (Kelong Chemical Reagent Factory, China) was dissolved at 98 °C, before 1 mL of the solution was added to 10 mL of the suspension containing 2.3 wt % of PMMA microsphere particles. Next, the prepared PMMA suspension was added to the TiO_2 colloid in terms of the TiO_2/PMMA mass ratios of 1: 0.1, 1: 0.2, 1: 0.4, 1: 0.6, respectively. After stirring for 12 h at room temperature, the mixed solution was sprayed on a glass slide. At last, the samples were calcined at 550 °C for 2 h, and the loadings of the TiO_2 porous thin films with pore formers (termed as TiO_2/PMMA porous thin film) were the same. Each mass ratio had two loadings of about 1.0 mg/cm^2 and 0.4 mg/cm^2. The former was used to measure the microstructural parameters while the later one was used to obtain the normal-hemispherical reflectance and transmittance, because the normal-hemispherical transmittance can only be measured when the thickness of the porous thin film is enough small. Note that given a catalyst loading, the change of the TiO_2/PMMA mass ratio can lead to the variation of the porosity. The larger mass ratio, the smaller porosity.

2.3 Measurements

After the preparation of the porous thin films, their optical and microstructure measurements were performed. The spectral normal-hemispherical reflectance and transmittance of the porous thin films were directly measured by ultraviolet-visible light (UV-VIS) spectrophotometer (PerkinElmer Lambda 950, USA) equipped with a 150-mm integrating sphere. All the TiO_2 porous thin films were illuminated by normal incident beam. The scanning wavelength range was from 300 nm to 800 nm and a blank glass slide was used as the baseline to eliminate the influence of the glass substrate. Every measurement was repeated three times at least to obtain the reliable data. Additionally, the field emission scanning electron microscope (TESCAN MIRA3) was used to obtain the cross-sectional morphologies and microstructures of the prepared porous thin films.

3 Results and Discussion

3.1 Morphologies of the Porous Thin Films

The cross-sectional morphologies of the prepared TiO_2 porous thin films are shown in Fig. 1. It can be seen that although the TiO_2 loadings were different, these porous thin films had similar porous structure with the pore size ranging from several nanometers to hundreds of nanometers (see Fig. 1). Using the cross-sectional views of these porous thin films, we also measured the thicknesses at different locations to estimate the average thickness. In this study, the thicknesses were about 5.3 μm,

9.9 μm, 20.7 μm and 31.0 μm corresponding to the TiO_2 loadings of about 0.5 mg, 1.0 mg, 2.0 mg and 3.0 mg, respectively. It can be found that the thickness of the porous thin film was almost linear with the TiO_2 loading. Therefore, it can be inferred that the porosity and the refractive index remain unchanged for these porous thin films. Based on the TiO_2 density and the measured thickness, the porosity of the TiO_2 porous thin film could be estimated to be about 74.3%. According to the relationship between the equivalent refractive index and the porosity of the porous media [19], the equivalent refractive index was estimated to be 1.572.

Figure 2 shows the morphologies of the cross-sectional views of the TiO_2/PMMA porous thin films with the loading of about 1.0 mg at various TiO_2/PMMA mass ratios. As can be seen from Fig. 2, after the PMMA particles were added, the pores with about 1 μm in diameter were randomly distributed inside the thin films,

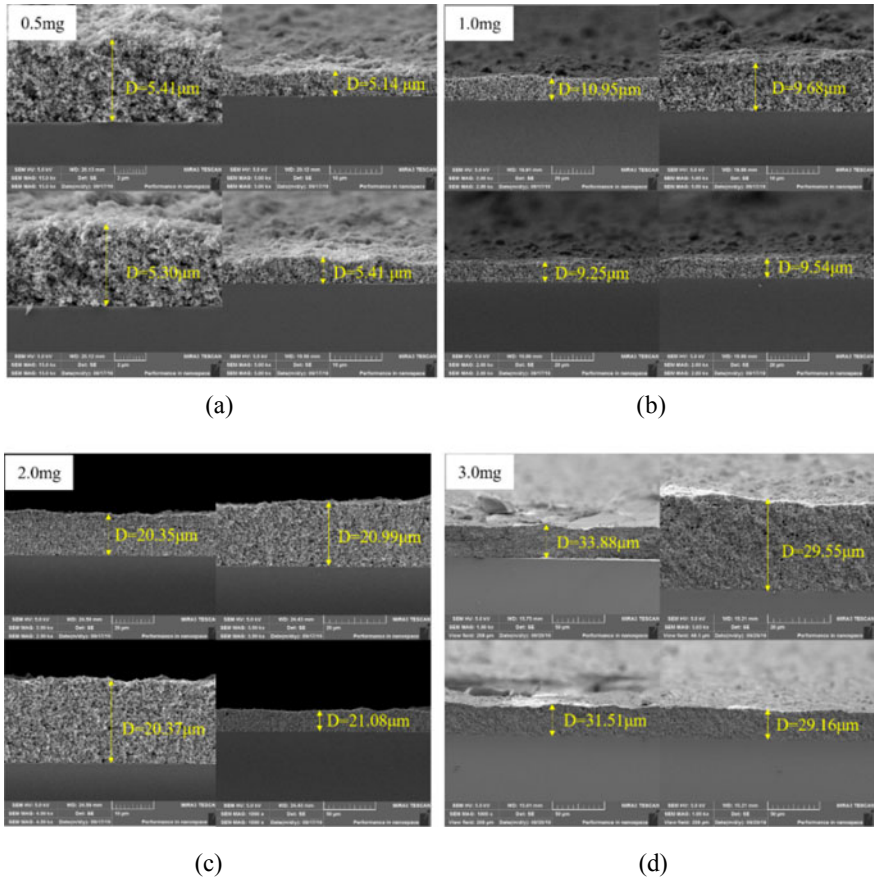

(a) (b)

(c) (d)

Fig. 1 Morphologies of the cross-sectional views of the TiO_2 porous thin films with different loadings: (a) 0.5 mg; (b) 1.0 mg; (c) 2.0 mg; (d) 3.0 mg

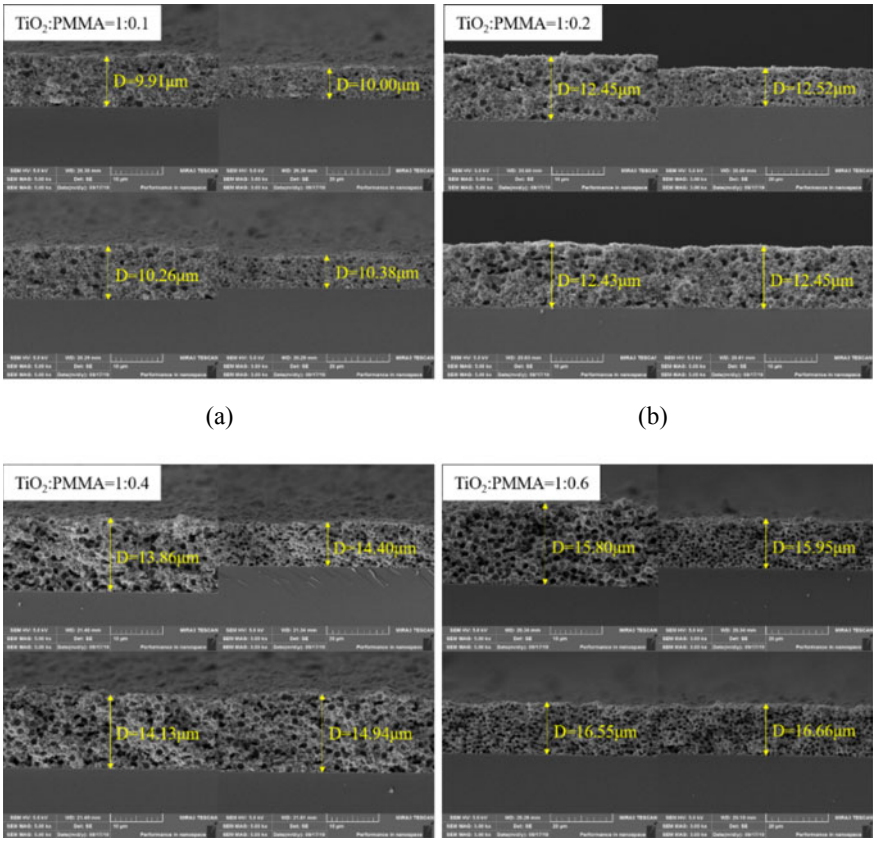

Fig. 2 Morphologies of the cross-sectional views of the TiO_2/PMMA porous thin films with different mass ratios: (a) TiO_2:PMMA = 1:0.1; (b) TiO_2:PMMA = 1:0.2; (c) TiO_2:PMMA = 1:0.4; (d) TiO_2:PMMA = 1:0.6

which were consistent with the diameter of the PMMA particles. This fact indicates that the PMMA particles can be successfully used as the pore former for the preparation of the TiO_2 porous thin films. Moreover, the pore density increased linearly with decreasing the TiO_2/PMMA mass ratio. This is because the decrease of the TiO_2/PMMA mass ratio led to more pore formers to be removed during the calcination, which then created more pores in the porous thin film. According to the cross-sectional images, the thicknesses of the TiO_2/PMMA porous thin films with the loading of about 1.0 mg were estimated to be about 10.1 μm, 12.5 μm, 14.3 μm, 16.2 μm, corresponding to the TiO_2/PMMA mass ratios of 1 : 0.1, 1 : 0.2, 1 : 0.4, 1 : 0.6, respectively. This result indicated that the porosity and thickness of the porous thin film rose with decreasing the mass ratio due to the increased pore volume. Finally, the thicknesses, porosities and equivalent refraction index of

various TiO_2/PMMA thin films were calculated and the results are listed in the Table 1. It can be seen that the equivalent refractive index of the TiO_2/PMMA porous thin film decreases with increasing the porosity.

3.2 *Reflectance and Transmittance of the Porous Thin Films*

Figure 3 presents the variations in the normal-hemispherical reflectance and transmittance of the TiO_2 porous thin film with the TiO_2 loading. It can be seen that in the ultraviolet spectrum, the normal-hemispherical reflectance of the TiO_2 porous thin film apparently decreased with decreasing the wavelength (see Fig. 3a). There was almost no reflection when the wavelength was below 350 nm. Similarly, the normal-hemispherical transmittance decreased with the decrease of the wavelength, dropping to zero at nearly 350 nm (see Fig. 3b). The reason is that TiO_2 has strong ability to absorb UV light. As the wavelength decreases and the photon energy gradually goes up, the TiO_2 porous thin films are able to absorb more photons so that the transmitted and reflected light significantly reduces. Moreover, the light attenuation increases with the thickness caused by the increased TiO_2 loading, so that the normal-hemispherical transmittance declines, as shown in Fig. 3b.

In the visible-light spectrum (400 nm−800 nm), the normal-hemispherical reflectance decreased whereas the normal-hemispherical transmittance increased with increasing the wavelength, as shown in Fig. 3a and 3b. This result indicates that the intensities of scattering and back-scattering decline when the wavelength increases. In addition, the light scattering in porous media increases due to the increased thickness. In this case, the directly transmitted light is weakened and the back scattering is enhanced. Therefore, the normal-hemispherical transmittance decreases while the normal-hemispherical reflectance increases.

Figure 4 shows the variations in the normal-hemispherical reflectance and transmittance of the TiO_2/PMMA porous thin film with the TiO_2:PMMA mass ratio. It can be seen that the variation trend of the normal-hemispherical reflectance and transmittance shows no significant difference between the TiO_2 and TiO_2/PMMA porous thin films, which can be confirmed by comparing Fig. 4 with Fig. 3.

Another finding is that the normal-hemispherical reflectance of the TiO_2/PMMA porous thin films with different mass ratios (i.e. various porosities, small mass ratio represents large porosity) almost remained identical in the UV spectrum (<390 nm), but increased with increasing the porosity in the visible-light spectrum. With the same TiO_2 loading, the normal-hemispherical transmittance of TiO_2/PMMA porous thin films decreased with increasing the porosity in the whole spectrum. The increase of the porosity could enhance the light scattering in the porous thin film in the visible spectrum, leading to the increase of the back-scattering. As a result, the reflectance increased due to the increase of back-scattering while the transmittance decreased.

Table 1 Microstructural parameters of the TiO_2/PMMA porous thin films

Sample	Average thickness (μm)	Pore volume (mm^3/mg)	Porosity	Refraction index
TiO_2	9.9	0.736	0.743	1.572
TiO_2:PMMA = 1:0.1	10.1	0.756	0.748	1.562
TiO_2:PMMA = 1:0.2	12.5	0.981	0.794	1.476
TiO_2:PMMA = 1:0.4	14.3	1.179	0.822	1.420
TiO_2:PMMA = 1:0.6	16.2	1.370	0.843	1.377

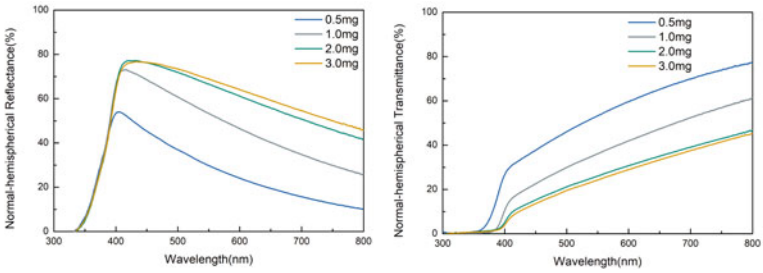

(a) (b)

Fig. 3 Variations in (a) the normal-hemispherical reflectance and (b) the normal-hemispherical transmittance of the TiO_2 porous thin film with the TiO_2 loading

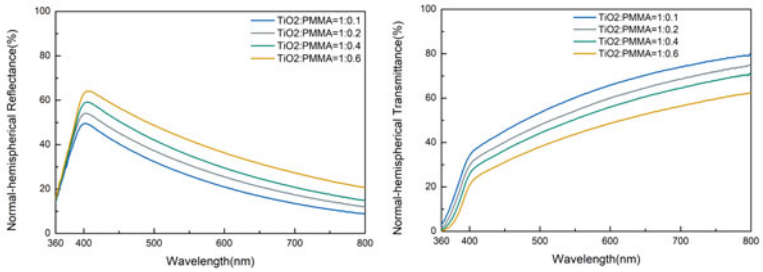

(a) (b)

Fig. 4 Variations in (a) the normal-hemispherical reflectance and (b) the normal-hemispherical transmittance of the TiO_2/PMMA porous thin film with the TiO_2:PMMA mass ratio

3.3 Absorption and Scattering Coefficients

Based on the porosity, equivalent refractive index and the measured normal-hemispherical reflectance and transmittance, the absorption coefficient and the scattering coefficient of the TiO_2 porous thin film could be retrieved by using the spectral element method [16]. It is worth noting that the thickness of the TiO_2 porous thin films should be enough thin to obtain the normal-hemispherical transmittance, so that the TiO_2 porous thin film with a loading of 0.5 mg was only calculated. The result is shown in Fig. 5. It is found that the absorption coefficient reduced sharply from 2703.5 cm^{-1} at 360 nm to 91.4 cm^{-1} at 400 nm and then becomes unchanged in the visible-light region. The reason is that TiO_2, as a semiconductor, whose band gap is 3.2 eV, can only absorb UV light. In the meantime, the absorption ability will increase with decreasing the wavelength. However, this is not the case for the scattering coefficient, which rose to the highest value of 9742.8 cm^{-1} at the wavelength of 378 nm and then dropped exponentially with an increase in the wavelength. It is noticeable that the absorption coefficient was 1692.3 cm^{-1} and the scattering coefficient was 8466.0 cm^{-1} at 365 nm, which are typically used in the photocatalytic fuel cells with TiO_2 as the photoanode.

Using the same approach, the radiative properties of the TiO_2/PMMA porous thin films can also be achieved, as shown in Fig. 6. It can be seen that as the wavelength increased, the trend of scattering coefficient and absorption coefficient of the TiO_2/PMMA porous thin films is the same as those of the TiO_2 porous thin films. For the absorption coefficient, although the increase of the porosity could slightly increase the absorption coefficient (see the inserted figure in Fig. 6a) in the ultraviolet spectrum (<390 nm), a noticeable increase for the scattering coefficient of the TiO_2/PMMA porous thin film could be observed with increasing the porosity. This phenomenon can be attributed to the increased surface due to the increase of pore volume, which effectively strengthens the surface reflection inside the porous

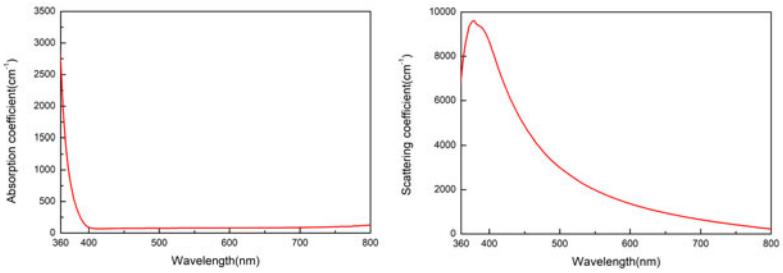

(a) (b)

Fig. 5 Radiative properties of the TiO_2 porous thin film: (a) absorption coefficient and (b) scattering coefficient

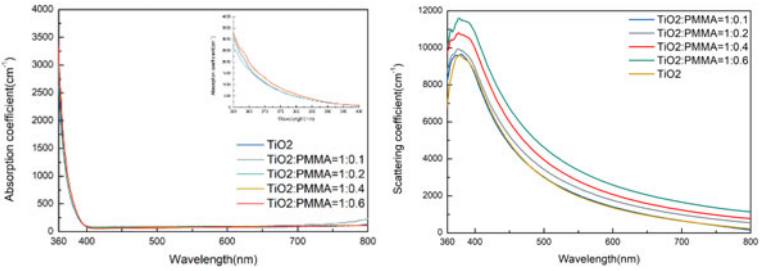

(a) (b)

Fig. 6 Radiative properties of the TiO_2/PMMA porous thin film: (a) absorption coefficient and (b) scattering coefficient

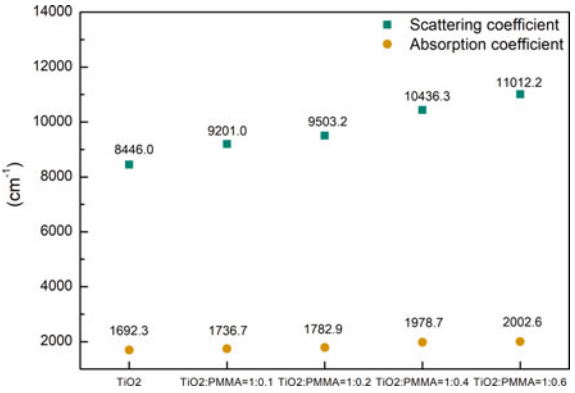

Fig. 7 Radiative properties of the TiO_2 and TiO_2/PMMA porous thin films at 365 nm

thin film. In this case, the increased scattering coefficient slightly enhanced the absorption. However, because the absorption coefficient is mainly dependent on the nature of TiO_2 properties, there was no significant difference between them.

Because TiO_2 can only respond to ultraviolet light and is usually illuminated at 365 nm for the TiO_2 photoanode, we particularly compared the absorption coefficient and scattering coefficient of the TiO_2 and TiO_2/PMMA porous thin films at this wavelength to examine the effect of the porosity, as shown in Fig. 7. It can be found that the increased porosity could efficiently enhance the light scattering in the TiO_2 porous thin film. Moreover, the scattering coefficient is five times more than the absorption coefficient. Therefore, proper design of the porous structure of the TiO_2 photoanode is critically important to improve the performance of the photocatalytic fuel cell.

4 Conclusions

In this paper, the radiative properties of the TiO_2 porous thin films were investigated in the ultraviolet spectrum and visible-light spectrum. We prepared the photoanodes with various loadings and porosities by using TiO_2 nanoparticles and the pore former of PMMA. The cross-sectional views of the porous thin films were characterized, by which the porosity and equivalent refractive index could be estimated. We also measured the normal-hemispherical reflectance and transmittance of the porous thin films. It was found that in the ultraviolet spectrum, the normal-hemispherical reflectance and transmittance of the porous thin film apparently decreased with decreasing the wavelength. The normal-hemispherical reflectance of the porous thin films was similar while the normal-hemispherical transmittance reduced as the TiO_2 loading and the porosity increased (the TiO_2:PMMA mass ratio decreased). In the visible-light spectrum, the normal-hemispherical reflectance decreased whereas the normal-hemispherical transmittance increased as the wavelength increased.

Based on the experimental results, the absorption coefficient and the scattering coefficient could be retrieved by the spectral element method. It is found that the absorption coefficient sharply decreased in the UV light region and then was almost unchanged. For the scattering coefficient, it firstly increased and then dropped. There existed a maximum scattering coefficient at the wavelength of about 378 nm. Moreover, the increase of porosity (the decrease of the TiO_2:PMMA mass ratio) obviously increased the scattering coefficient of the porous thin films, while slight rise occurs for the absorption coefficient. The obtained radiative parameters of the TiO_2 porous thin film can be used to develop more accurate transport model for the photoanode.

Acknowledgements The authors gratefully acknowledge the financial supports of the National Natural Science Foundation of China (No. 51925601, No. 51620105011 and No. 51776026), the Program for Back-up Talent Development of Chongqing University (No. CQU2017HBRC1A01) and the Fundamental Research Funds for the Central Universities (No. 2018CDXYDL0001).

References

1. Antoniadou, M., Vaiano, V., Sannino, D., Lianos, P.: Photocatalytic oxidation of ethanol using undoped and Ru-doped titania: acetaldehyde, hydrogen or electricity generation. Chem. Eng. J. **224**, 144–148 (2013)
2. Du, Z., Li, H., Gu, T.: A state of the art review on microbial fuel cells: a promising technology for wastewater treatment and bioenergy. Biotechnol. Adv. **25**(5), 464–482 (2007)
3. Logan, B.E.: Exoelectrogenic bacteria that power microbial fuel cells. Nat. Rev. Microbiol. **7** (5), 375–381 (2009)
4. Liu, H., Cheng, S., Logan, B.E.: Production of electricity from acetate or butyrate using a single-chamber microbial fuel cell. Environ. Sci. Technol. **39**(2), 658–662 (2005)
5. Padoin, N., Soares, C.: An explicit correlation for optimal TiO_2 film thickness in immobilized photocatalytic reaction systems. Chem. Eng. J. **310**, 381–388 (2017)

6. Chang, H.T., Wu, N.M., Zhu, F.: A kinetic model for photocatalytic degradation of organic contaminants in a thin-film TiO_2 catalyst. Water Res. **34**(2), 407–416 (2000)
7. Khataee, A.R., Fathinia, M., Aber, S.: Kinetic modeling of liquid phase photocatalysis on supported TiO_2 nanoparticles in a rectangular flat-plate photoreactor. Ind. Eng. Chem. Res. **49** (24), 12358–12364 (2010)
8. Tournat, V., Pagneux, V., Lafarge, D., Jaouen, L.: Multiple scattering of acoustic waves and porous absorbing media. Phys. Rev. E **70**(2), 026609–026619 (2004)
9. Makino, T., Kunitomo, T., Sakai, I., Kinoshita, H.: Thermal radiation properties of ceramic materials. Heat Transfer-Japanese Res. **13**, 33–50 (1984)
10. Molenaar, R., Jaap, J., Zijp, J.R.: Determination of Kubelka-Munk scattering and absorption coefficients by diffuse illumination. Appl. Opt. **38**(10), 2068–2077 (1999)
11. Pickering, J.W., Prahl, S.A., Van Wieringen, N., Beek, J.F., Sterenborg, H.J., Van Gemert, M. J.: Double-integrating-sphere system for measuring the optical properties of tissue. Appl. Opt. **32**(4), 399–410 (1993)
12. Cheong, W.F., Prahl, S.A., Welch, A.J.: A review of the optical properties of biological tissues. IEEE J. Quantum Electron. **26**(12), 2166–2185 (1990)
13. Petrasch, J., Wyss, P., Steinfeld, A.: Tomography-based Monte Carlo determination of radiative properties of reticulate porous ceramics. J. Quant. Spectr. Radiative Transf. **105**(2), 180–197 (2007)
14. Xie, B.W., Ma, L.X., Zhao, J.M., Liu, L.H., Wang, X.Z., He, Y.R.: Experimental study of the radiative properties of hedgehog-like ZnO–Au composite particles. J. Quant. Spectr. Radiative Transf. **232**, 93–103 (2019)
15. Morales, J.J., Nuevo, M.J.: A general method for calculating reflection and transmission coefficients in multiple slabs. Am. J. Phys. **59**(12), 1140–1143 (1991)
16. Zhao, J.M., Liu, L.H.: Least-squares spectral element method for radiative heat transfer in semitransparent media. Numer. Heat Transf. Part B Fundam. **50**(5), 473–489 (2006)
17. Li, L., Wang, G., Chen, R., Zhu, X., Wang, H., Liao, Q., Yu, Y.: Optofluidics based micro-photocatalytic fuel cell for efficient wastewater treatment and electricity generation. Lab Chip **14**(17), 3368–3375 (2014)
18. Li, L., Chen, R., Zhu, X., Liao, Q., Wang, H., An, L., Zhang, M.: A cascading gradient pore microstructured photoanode with enhanced photoelectrochemical and photocatalytic activities. J. Catal. **344**, 411–419 (2016)
19. Yang, Z., Zhu, D., Lu, D.: The relationship between porous ratio and refractive index in nanoporous film. Acta Optica Sinica **23**(11), 1366–1369 (2003)